

Video Article

Dissection, MicroCT Scanning and Morphometric Analyses of the Baculum

Nicholas G. Schultz¹, Erik Otárola-Castillo², Matthew D. Dean¹¹Molecular and Computational Biology, University of Southern California (USC)²Purdue UniversityCorrespondence to: Matthew D. Dean at matthew.dean@usc.eduURL: <https://www.jove.com/video/55342>DOI: [doi:10.3791/55342](https://doi.org/10.3791/55342)

Keywords: Bioengineering, Issue 121, Morphometrics, semi-landmark, 3d, computational geometry, Generalized Procrustes Analysis, baculum

Date Published: 3/19/2017

Citation: Schultz, N.G., Otárola-Castillo, E., Dean, M.D. Dissection, MicroCT Scanning and Morphometric Analyses of the Baculum. *J. Vis. Exp.* (121), e55342, doi:10.3791/55342 (2017).

Abstract

Modern morphometrics provides powerful methods to quantify size and shape variation. A basic requirement is a list of coordinates that define landmarks; however such coordinates must represent homologous structures across specimens. While many biological objects consist of easily identified landmarks to satisfy the assumption of homology, many lack such structures. One potential solution is to mathematically place semi-landmarks on an object that represent the same morphological region across specimens. Here, we illustrate a recently developed pipeline to mathematically define semi-landmarks from the mouse baculum (penis bone). Our methods should be applicable to a wide range of objects.

Video Link

The video component of this article can be found at <https://www.jove.com/video/55342/>

Introduction

The field of morphometrics includes a diversity of methods to quantify the size and shape of the biological form, a fundamental step in scientific inquiry^{1,2,3,4,5,6}. Traditionally, the statistical analysis of size and shape begins by identifying landmarks on a biological structure, and then measuring linear distances, angles and ratios, which could be analyzed in a multivariate framework. Landmark-based Geometric Morphometrics is an approach that retains the spatial position of landmarks, preserving geometric information from data collection through analysis and visualization⁵. Generalized Procrustes Analysis (GPA) can be applied to remove variation in location, scale, and rotation of landmarks to produce an alignment between specimens that minimizes their squared differences - what remains is shape dissimilarity⁷.

An important concept of any morphometric analysis is homology, or the idea that one can reliably identify landmarks representing biologically meaningful and discrete features that correspond between specimens or structures. For example, human skulls have homologous processes, foramina, sutures, and ducts that can enable morphometric analyses. Unfortunately, the identification of corresponding landmarks is difficult across many biological structures, especially those with smooth surfaces or curves^{8,9,10}.

We approach this problem below using computational geometry. The general workflow is to generate a three dimensional scan of the object that can be represented as a cloud of points, and then rotate and transform that point cloud so that all specimens are oriented on a common coordinate system. Then we mathematically define semi-landmarks from specific regions of the object. Discrete semi-landmarks placed on such regions are biologically arbitrary¹¹. Conducting GPA and subsequent statistical analyses can produce undesirable artifacts^{8,12} because arbitrarily placed landmarks may not be biologically homologous. Therefore, we allow these semi-landmarks to mathematically "slide". This procedure minimizes the potential difference between structures. As argued elsewhere the sliding algorithm used here is appropriate to quantify similar anatomical regions lacking easily identified corresponding landmarks^{3,6,8,10,11,12}. These methods have their limitations¹³, but should be adaptable to objects of different size and shape.

Here, we illustrate how this method was applied in a recent study of the mouse baculum¹⁴, a bone in the penis that has been gained and lost multiple independent times during mammalian evolution¹⁵. We discuss the dissection and preparation of a specific bone, the baculum (Protocol 1), the generation of microCT images (Protocol 2), and the conversion of these images to a format that enables all downstream computational geometry (Protocols 3 and 4). After these steps, each specimen is represented by ~100K x-y-z coordinates. We then walk through a series of transformations that effectively align all specimens into a common orientation (Protocol 5), then define semi-landmarks from aligned specimens (Protocol 6). Protocols 1-4 should be similar regardless of the object being analyzed. Protocol 5 and Protocol 6 are specifically designed for a baculum, but it is our hope that by detailing these steps, investigators can imagine modifications that would be relevant for their object of interest. For example, modifications of these methods were applied to study whale pelvic bones and rib bones¹⁶.

Protocol

All procedures and personnel were approved by the University of Southern California's Institute for Animal Care and Use Committee (IACUC), protocol #11394.

1. Baculum Dissection and Preparation

1. Euthanize a sexually mature male mouse via carbon dioxide over-exposure, according to protocols set forth by the relevant Institutional Animal Care and Use Committee (IACUC).
2. Lay the animal in the supine position, and protract the penis by applying pressure with thumbs lateral to the preputial opening.
3. Once the penis is protracted, extend the tissue through the prepuce as far as possible.
4. With scissors, cut the penile body proximal to the glans penis where the baculum resides.
5. Transfer the dissected penis to a 1.7 mL tube and add 200 μ L tap water. Make certain that the penis is fully submerged in the liquid.
6. Incubate the tissue in water at \sim 50 $^{\circ}$ C for 3-5 days.
7. After proper incubation, remove the surrounding tissue from the baculum, using forceps under a dissection microscope. Gently squirt 70% ethanol to push off remaining tissue and clean the bone.
8. Place the dissected baculum into a new microcentrifuge tube with the cap open. Leave cap open O/N to dry out bone.

2. MicroCT Scanning

1. Press a microCT scan cylindrical holder into a brick of florist foam to create a cylinder of florist foam.
2. Extract the cylinder of florist foam and cut slices \sim 2-5 cm thick.
3. Push dried bacula into the florist foam, around the periphery of an individual slice to minimize interference during scanning. The precise orientation of bones should be remarked allowing for proper identification of individual specimens in Protocol 4.
4. Gently place the slice with the embedded bones into the microCT holder.
5. Acquire microCT scans. In the case of mouse bacula¹⁴, we used a uCT50 scanner (Scanco Medical AG, Bruttisellen, Switzerland) at the USC Molecular Imaging Center under the following settings: 90 kVp, 155 μ A, 0.5 mm Al filter, 750 projections per 180 (360 coverage), exposure time of 500 ms, and voxel size of 15.5 mm.

3. MicroCT Processing: Converting a .DCM Stack to a Single .xyz File

NOTE: Each microCT scan produces a stack of .DCM, or "dicom", files that represent image slices taken through the object. All downstream computational geometry requires flat .xyz files, which is simply a text file that contains four columns – the x, y, and z coordinates of each pixel, and the intensity of the pixel, ranging from -5,000 (black) to +5,000 (white). A pixel threshold above 3,000 generally works well as a threshold for defining bones.

1. Install Python (www.python.org) and the PYTHON modules COMMANDS, DICOM, PYLAB, SYS, and NUMPY.
2. Open "01_process_dicom.py"{Figshare} with any text editor. Under the Variables section, change path, pixel thresholds, and directory names as necessary.
3. Run "python 01_process_dicom.py". Progress will be printed to screen. Within each directory named in step 3.2, a new file is made named; for example, directory_name.PT3000.xyz, where PT3000 indicates the pixel threshold indicated in step 3.2.

4. MicroCT processing: Segmenting-out Individual Specimen .xyz Files

1. Install R (<https://www.r-project.org/>) with the library RGL.
2. Open the file '02_segment_dicoms.r'{Figshare} with any text editor. Under the Variables section, change the path name to point to the .xyz file created in Protocol 3 above.
3. From within R, run the command "source('02_segment_dicoms.r') (without the double quotes).
4. After the three dimensional image of the .xyz file created in Protocol 3 appears, enter the number of specimens in the overall .xyz file. Then label and select the points from each specimen using the scroll and zoom functions.
NOTE: In the background, separate .xyz files will be made for each specimen. These appear in a directory named, for example, XYZ_FILES_PT3000, where PT3000 indicates the pixel threshold used.

5. "Aligning" Specimen .xyz Files to Common Coordinates.

1. Open the Python script "03_transform.py"{Figshare}, which requires the additional module mattdean_modules.py{Figshare}, as well as two self-standing applications: "rotate_translate_cylindrical" (https://github.com/timydaley/dean_cylindrical_tranform) and "qconvex" (www.qhull.org/html/qconvex.htm) that are used by this script.
2. Under the Variables section, identify the full path names to mattdean_modules.py, rotate_path and qconvex_dir. In addition, identify the full path to the directory containing the individual .xyz files created in step 4.
3. Run 03_transform.py, which creates a new file per specimen with the suffix .TRANSFORMED.xyz.

6. "Slicing" Aligned Specimen .xyz Files to Identify Semi-landmarks.

1. Open and run the Python script "04_identify_landmarks.py" (Figshare). In the Variables section, identify full path names to the directory containing the .TRANSFORMED.xyz files. This script identifies 802 semi-landmarks that can be used to quantify size and shape of the structure.

Representative Results

The x-y-z coordinates of the semi-landmarks produced in Protocol 6 can be directly imported into any landmark-based geometric morphometrics analysis¹⁷. The computational pipeline above has been applied to study mouse bacula¹⁴, as well as whale pelvic and rib bones¹⁶. More details on the computational definition of semi-landmarks are presented here, in an attempt to help researchers visualize steps that might be modified to accommodate their particular object of interest. The baculum contains several unique features that were exploited to automate certain transformations. For example, after computationally cutting the bone into two halves along a proximal-distal axis, we identified the proximal half simply by comparing the total number of points (the proximal has more). As long as there exist unique features such as this, our methods should be adaptable to any object. In addition, it should be emphasized that we empirically determined certain thresholds, such as "10% proximal" that performed well in our baculum studies, but most certainly need to be reassessed for other objects.

Beginning in Protocol 5, the first computational step is to calculate the convex hull (the smallest set of points that contains all other points in a sample) to identify the two points that are furthest apart from each other. These two points (red spheres, **Figure 1C**) begin to define a new z-axis (red line, **Figure 1C**) that runs proximal-distal through the bone. In the case of the baculum, the half of the point cloud that contains more points is defined as the proximal end.

Second, the entire point cloud is transformed so that the proximal point takes on the x,y,z coordinates of 0,0,0 and the distal point takes on the x,y,z coordinates of 0,0,+z, where +z is some positive value dependent on the size of the bone. At the end of this step, a z-axis passes through the length of the bone. For procedures below, the length from the minimum to maximum z-coordinates will be referred to as Zlength.

Third, to correct for variance associated with the exact placement of the proximal and distal points identified above, the 10% most proximal and 10% most distal points are sampled separately (**Figure 1D**), their respective centroids identified (red spheres, **Figure 1E**) and the point cloud transformed such that the proximal centroid is 0,0,0, and the distal centroid is 0,0,+z, with a new z-axis that passes through the center of the specimen (red line, **Figure 1E**).

Fourth, the point cloud is rotated around the z-axis by first taking a slice of points in the proximal 15 to 15.25% Zlength of the structure (blue points, **Figure 1E**). This slice of points is flattened in the z dimension (*i.e.* z-coordinates are simply ignored), the convex hull taken, and the minimum bounding rectangle (the smallest rectangle that contains all other points) calculated. Imagine a line connecting the midpoints of the two short sides of this minimum bounding rectangle. We rotate the point cloud until these two midpoints become -x,0,+z and +x,0,+z, respectively, thus this line becomes a new x-axis. After transformation, the distance between the maximal and minimal x values are referred to as Xlength. A new file is created from specimen.xyz to specimen.TRANSFORMED.xyz.

Fifth, points within 1% Xlength of the z-axis are sliced out (blue points, **Figure 1F**), and the single most proximal and single most distal point identified from this central slice and labeled DISTAL and PROXIMAL, respectively. These are the first two semi-landmarks identified.

Sixth, 50 evenly spaced slices of points are sampled along the z-axis (red points, **Figure 1G**). Each slice is a thickness of 1% Zlength. Each slice is then flattened in the z dimension, and divided equally by 7 vertical lines (red lines, **Figure 1H**). Points within 2% Xlength of each line are kept (red points, **Figure 1H**), then the points with the maximum and minimum y-coordinate are kept, projected onto each respective line, and labeled VENTRAL and DORSAL, respectively. In addition, labels contain the slice number and the line number, for example P15_VENTRAL4 is the ventral point sampled from the 4th vertical line of the 15th slice. Importantly, every point labeled, for example, P15_VENTRAL4, occurs once and only once across all specimens, preserving correspondence. In addition to the ventral and dorsal points of each of the 7 lines (14 semi-landmarks total), the points with the maximum and minimum x-value are sampled and labeled LEFT and RIGHT, respectively. The y and z coordinates of LEFT and RIGHT are smoothed using the lowess function in R. For the baculum, a total of 16 semi-landmarks are defined per slice (red spheres, **Figure 1H**); with 50 slices plus the PROXIMAL and DISTAL semi-landmarks defined above, 802 semi-landmarks are sampled per specimen (green spheres, **Figure 1I**). All other points from the original microCT scan are discarded.

It should be noted that although ventral/dorsal and proximal/distal polarity was determined mathematically, all specimen alignments were visually confirmed and manually adjusted as required. In our sample of 369 bacula, approximately 10 had to be manually adjusted.

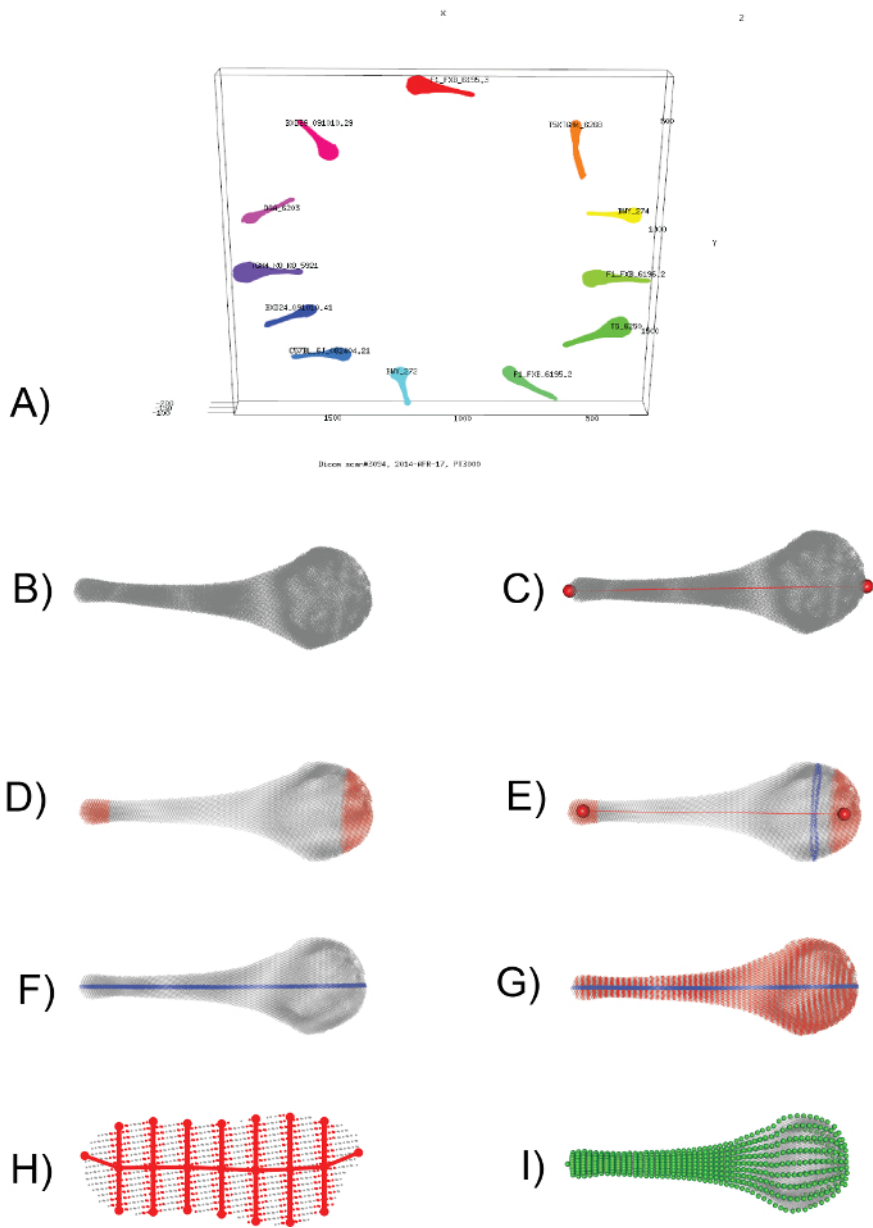


Figure 1: Visual Representation of the Computational Workflow (Protocol 4-6). (A) A screenshot from the 02_segment_dicoms.r script (Protocol 4), showing the assignment of distinct point clouds to individual specimens. (B) Enlarged view of one baculum, represented by a cloud of ~100K x-y-z points. (C) Identification of the two points furthest apart from each other (red spheres), used to define a new z-axis that runs proximal-distal through the bone (red line). (D) Sampling the proximal-most 10% and distal-most 10% of points (red points) provides a means to adjust for slight variance in the exact placement of the z-axis. (E) The centroids of the proximal-most 10% and distal-most 10% (red spheres) are used to define a new z-axis (red line). Then, a slice of points falling between 15.00-15.25% of this new z-axis (blue points) is taken to calculate the minimum bounding rectangle. The point cloud is rotated until the long side of the minimum bounding rectangle is parallel to a new x-axis. (F) a slice of points running along the midline (blue points) is sampled and the proximal-most and distal-most point defined as a semi-landmark. (G) 50 evenly spaced slices of points are sampled (red points), with (H) showing one such slice. 16 points (red circles) are defined to capture the outline of each slice. (I) When repeated across all slices, a total of 802 semi-landmarks (green spheres) define the structure and are used in all downstream morphometric applications. [Please click here to view a larger version of this figure.](#)

Discussion

The critical steps in the above protocol are 1) dissecting the bacula, 2) gathering the microCT images, 3) converting the microCT output to a flat file of x-y-z coordinates, 4) segmenting out each specimen's point cloud, 5) transforming each specimen to a standardized coordinate system, and 6) defining semi-landmarks. These steps are easily modified to accommodate different objects.

These methods can likely be applied to any object that is essentially "rod-shaped", or at least not too curved. Objects that curve back on themselves to become "u-shaped" cannot be currently analyzed, because slicing (**Figure 1G**) would return points from different parts of the object. Such objects could be accommodated in the future by computationally straightening the object prior to slicing.

We have presented a general method for mathematically defining semi-landmarks from shapes that lack solid landmarks. These general methods have been modified to study the evolution of whale pelvic and rib bones¹⁶, which have very different shapes. Our computational methods for defining landmarks should be applicable to any series of x-y-z coordinates. We employed microCT scanning here, given the small size of mouse bacula¹⁴. For larger bones, such as the whale pelvic and rib bones, we employed a laser scanner that reconstructed the surface of the bones¹⁶. It is important to visually inspect all sets of semi-landmarks to verify the quality of the method. The main advantage of our computational methods is that they precisely quantify the size and shape variation, and preserve the correspondence between distinct regions of the object.

Disclosures

The authors declare that they have no competing financial interests.

Acknowledgements

Tim Daley and Andrew Smith provided many useful computational discussions during the early days; Tim Daley wrote the program `rotate_translate_cylindrical` necessary for Protocol 5. Computational resources were provided by the High Performance Computing Cluster at the University of Southern California. This work was supported by NIH grant #GM098536 (MDD).

References

1. Slice, D. E. Geometrics morphometrics. *Annu. Rev. Anthropol.* **36** 261-281 (2007).
2. Slice, D. E. *Modern morphometrics in physical anthropology*. Vol. 6. Springer. (2005).
3. Zelditch, M. L., Swiderski, D. L., & Sheets, H. D. *Geometric morphometrics for biologists: a primer*. 2nd edn. Elsevier. (2012).
4. Bookstein, F. *Morphometric tools for landmark data: geometry and biology*. Cambridge University Press. (1991).
5. Rohlf, F. J., & Marcus, L. F. A Revolution in Morphometrics. *Trends. Ecol. Evol.* **8** (4), 129-132 (1993).
6. Zelditch, M. L., Swiderski, D. L., Sheets, H. D., & Fink, W. L. *Geometric morphometrics for biologists: a primer*. Elsevier. (2004).
7. Rohlf, F. J., & Slice, D. E. Extensions of the Procrustes method for the optimal superimposition of landmarks. *Syst. Zool.* **39** (1), 40-59 (1990).
8. Gunz, P., & Mitteroecker, P. Semilandmarks: a method for quantifying curves and surfaces *Hystrix.* **24** (1), 103-109 (2013).
9. Gunz, P., Ramsier, M., Kuhrig, M., Hublin, J. J., & Spoor, F. The mammalian bony labyrinth reconsidered, introducing a comprehensive geometric morphometric approach. *J. Anat.* **220** (6), 529-543 (2012).
10. Mitteroecker, P., & Gunz, P. Advances in geometric morphometrics. *Evol. Biol.* **36** (2), 235-247 (2009).
11. Bookstein, F. J. Landmark methods for forms without landmarks: morphometrics of group differences in outline shape. *Med. Im. Anal.* **1** (3), 225-243 (1997).
12. Gunz, P., Mitteroecker, P., & Bookstein, F. in *Modern morphometrics in physical anthropology*. (ed Dennis E Slice) 73-98 Kluwer Press, (2005).
13. Oxnard, C., & O'Higgins, P. Biology Clearly Needs Morphometrics. Does Morphometrics Need Biology? *Biological Theory.* **4** (1), 84-97 (2009).
14. Schultz, N. G. *et al.* The genetic basis of baculum size and shape variation in mice. *G3.* **6** (5), 1141-1151 (2016).
15. Schultz, N. G., Lough-Stevens, M., Abreu, E., Orr, T. J., & Dean, M. D. The baculum was gained and lost multiple times during mammalian evolution. *Integr Comp Biol.* **icw034** (2016).
16. Dines, J. P. *et al.* Sexual selection targets cetacean pelvic bones. *Evolution.* **68** (11), 3296-3306 (2014).
17. Adams, D. C., & Otárola-Castillo, E. geomorph: an R package for the collection and analysis of geometric morphometric shape data. *Methods Ecol. Evol.* **4** (4), 393-399 (2013).